Journal of Hydrology 666 (2026) 134785

Contents lists available at ScienceDirect

Journal of Hydrology

journal homepage: www.elsevier.com/locate/jhydrol

Synergistic effects of climate forcings from three oceans on the reserve of "Atmospheric water tower" over the Tibetan Plateau

Pengjie Ren [a,b], Wusheng Yu [a,*], Stephen Lewis [c], Yaoming Ma [a,b,d,*], Yuanyuan Dang [a,b], Lei Zhong [e,*], Zhuanxia Zhang [a,b], Yong Liu [f,*], Lun Luo [g,h], Zhaowei Jing [i], Jingyi Zhang [j], Rong Guo [a,b], Qiaoyi Wang [a,b], Ziran Lei [a,b]

[a] State Key Laboratory of Tibetan Plateau Earth System, Environment and Resources (TPESER), Institute of Tibetan Plateau Research, Chinese Academy of Sciences, Beijing 100101, China
[b] University of Chinese Academy of Sciences, Beijing 100049, China
[c] Catchment to Reef Research Group, Centre for Tropical Water and Aquatic Ecosystem Research, James Cook University, Townsville, QLD 4811, Australia
[d] College of Atmospheric Science, Lanzhou University, Lanzhou 730000, China
[e] School of Earth and Space Sciences, University of Science and Technology of China, Hefei 230026, China
[f] Department of Atmospheric Science, School of Environmental Studies, China University of Geosciences, Wuhan, China
[g] Research Center of Applied Geology of China Geological Survey, Chengdu 610036, China
[h] Center for the Pan-Third Pole Environment, Lanzhou University, Lanzhou 730000, China
[i] School of Ecology and Nature Conservation, Beijing Forestry University, Beijing 100083, China
[j] College of Tourism, Henan Normal University, Xinxiang 453007, China

ARTICLE INFO

This manuscript was handled by Emmanouil Anagnostou, Editor-in-Chief

Keywords:
Reserve
Water vapor flux
Atmospheric water tower
Tibetan Plateau

ABSTRACT

The water vapor reserve over the Tibetan Plateau, known as the "atmospheric water tower," significantly influences the spatial patterns and trends of surface water resources in the region and surroundings. However, the reserve of the "atmospheric water tower" has not been precisely quantified, and how climate forcings from three oceans (i.e., the North Atlantic, Indian, and Pacific Oceans) influence variations in the reserve remain unclear. Here, we investigate interannual variations in the reserve over the Tibetan Plateau during 1951–2022 using ERA5 data. The results show that the climatological mean reserve of the "atmospheric water tower" is $(25.76 \pm 3.83) \times 10^6$ kg s^{-1} and the reserve gradually decreased from 1951 to 1973, but gradually increased after 1973. A major shift of the Atlantic Multidecadal Oscillation (AMO) around 1973 coincides with this trend of the reserve. We further demonstrate that climatic forcings including AMO, Indian Ocean Basin-Wide (IOBW), and El Niño-Southern Oscillation (ENSO) jointly drive the increasing trend in the reserve after 1973; however, the effect of the AMO on the reserve became relatively weaker after 1994 as the influence of ENSO became stronger. Clearly, the dominant climatic forcing for the increasing trend of the reserve has gradually changed from the North Atlantic Ocean to the Pacific Ocean over time. Our findings reveal a previously unrecognized transition in the dominant climate forcings for the reserve, moving beyond a static view to a dynamic one. We provide a new framework for predictions of regional climate and water resource changes under global warming.

1. Introduction

The moisture resource stored in the atmosphere over the Tibetan Plateau is known as the "atmospheric water tower" (Xu et al., 2008; Xu et al., 2014). This water vapor resource is vital due to its significant influence on precipitation (Xu et al., 2014; Zhang et al., 2017a; Ma et al., 2018; Liu et al., 2021) and surface water resources (Li et al., 2022a; Wang et al., 2022) across the Tibetan Plateau. The Tibetan Plateau is situated within the headwaters of several major Asian rivers (Immerzeel et al., 2010; Bolch et al., 2012), including the Yangtze, Yellow, Salween, and Mekong Rivers, which support almost two billion people in China and other downstream countries. Moreover, the water vapor over the Tibetan Plateau significantly affects the surrounding areas (Zhao et al., 2016; Wan et al., 2017; Zhu et al., 2021; Jia et al., 2025). Hence,

* Corresponding authors at: State Key Laboratory of Tibetan Plateau Earth System, Environment and Resources (TPESER), Institute of Tibetan Plateau Research, Chinese Academy of Sciences, Beijing 100101, China.
E-mail addresses: yuws@itpcas.ac.cn (W. Yu), ymma@itpcas.ac.cn (Y. Ma), zhonglei@ustc.edu.cn (L. Zhong), liuyong78@cug.edu.cn (Y. Liu).

https://doi.org/10.1016/j.jhydrol.2025.134785
Received 7 July 2025; Received in revised form 8 December 2025; Accepted 10 December 2025
Available online 13 December 2025

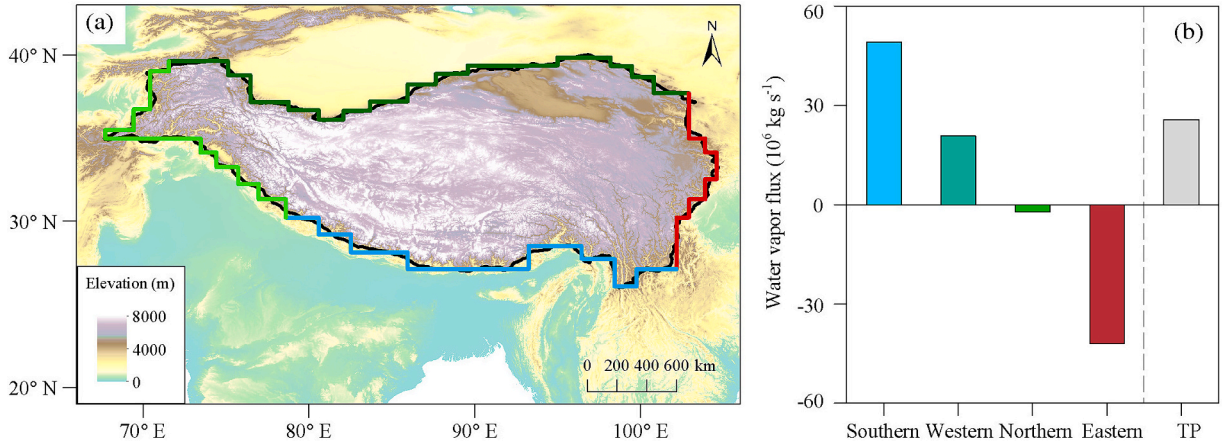

Fig. 1. (a) The boundaries of the Tibetan Plateau. The red, sky blue, grass green, and dark green solid lines represent the eastern, southern, western, and northern boundaries of the Tibetan Plateau, respectively. (b) The climatological annual mean water vapor flux across each boundary and reserve of the "atmospheric water tower" over the Tibetan Plateau over 1951–2022. The negative values indicate that water vapor flows out from the Tibetan Plateau. (For interpretation of the references to colour in this figure legend, the reader is referred to the web version of this article.)

determining the climatological mean and interannual variations of the net water vapor budget over the Tibetan Plateau are critical to quantify the total resource as well as to understand the dynamics that drive it (hereafter the net water vapor budget is defined as the reserve of the "atmospheric water tower").

The majority of previous studies have primarily focused on the reserve of the "atmospheric water tower" during the summer season whereby the estimates show considerable variability (Lin et al., 2016; Zhou et al., 2019; Xu et al., 2020; He et al., 2021; Zhao and Zhou, 2021; Li et al., 2022b; Sun et al., 2022; Wang and Zhao, 2022; Yu et al., 2022; Wang et al., 2024). For example, the summer reserves calculated by Lin et al. (2016) and Zhao and Zhou (2021) are 411×10^6 kg s^{-1} and 31.1×10^6 kg s^{-1}, respectively, a 13.2 fold difference. Similarly, the climatological mean reserve over the Tibetan Plateau also produced considerably different results where the mean reserve calculated by Yan et al. (2020) was 2.8 times higher than Xu et al. (2020). Hence, both the seasonal (summer) and climatological reserves of the "atmospheric water tower" are highly uncertain and the reasons for these highly variable estimates remain unclear.

Calculating the reserve of "atmospheric water tower" is centered on input and output budgets for the four boundaries of the Tibetan Plateau (eastern, southern, western, and northern boundaries). The four boundaries can be identified as input boundaries or output boundaries according to their different effects on the reserve. It is crucial to accurately identify the primary input or output boundary. By identifying the primary input or output boundary we can then analyze the main drivers that influence variations in the "atmospheric water tower" reserve. Regarding the climatological mean of the reserve, most scientists argued that the primary input boundary is the southern boundary, and the primary output boundary is the eastern boundary (Lin et al., 2016; Zhou et al., 2019; Yan et al., 2020; Li et al., 2022b; Yu et al., 2022). However, Xu et al. (2020) argued that the primary input boundary is the western boundary. These controversies prompt us to identify the input and output boundaries for the assessment of the "atmospheric water tower" reserve.

Several climate forcings likely drive the interannual variations in the reserve of the "atmospheric water tower" over the Tibetan Plateau (Gao et al., 2013, 2014; Zhang et al., 2017b; Meng et al., 2020; Sun et al., 2020; Chen et al., 2022a; Chen et al., 2022b). Most studies have focused on the impact of a singular forcing around the Tibetan Plateau to explain the interannual variations in the reserve. For example, Zhou et al. (2019) proposed that the decrease (increase) in the reserve over the Tibetan Plateau is closely associated with cyclones (anticyclones) over Lake Baikal. Yang et al. (2022) stated that the westward extension of the West Pacific Subtropical High can enhance the convergence of upper-level water vapor from the Bay of Bengal toward the Tibetan Plateau, leading to an increase in the reserve. Other studies have investigated the impacts of the remote and singular climate forcings on the dry/wet changes over the Tibetan Plateau. For instance, Sun et al. (2020) found that the summer wetting of the Tibetan Plateau is linked to the weakening of the westerlies caused by the positive phase of the Atlantic Multidecadal Oscillation Index (AMO). A recent study has pointed out that Atlantic oceanic droughts threaten the sustainability of the Tibetan Plateau. The study argues that the southern Tibetan Plateau has become more arid during 2003–2016 and that drought conditions have persistently expanded northward since 2009 (Zhang et al., 2023). However, this conclusion has been refuted by Zhao et al. (2025), who argued that Zhang et al. (2023) overstated the role of the Atlantic oceanic droughts in the water resource of the Tibetan Plateau. In fact, the combined effects of climate forcings from three oceans (i.e., the North Atlantic, Indian, and Pacific Oceans) on the reserve of "atmospheric water tower" over the Tibetan Plateau have not previously been explored. Importantly, whether the contributions of the dominant forcings to the "atmospheric water tower" reserve have changed over time and space also remains unclear. These issues motivate us to thoroughly explore the mechanisms that cause interannual variations in the reserve of the "atmospheric water tower" over the Tibetan Plateau.

This study applies the fifth generation European Centre for Medium-Range Weather Forecasts (ERA5) reanalysis for the period 1951–2022 to address the above-mentioned research gaps on the reserve of the "atmospheric water tower." First, we precisely quantify the climatological mean reserve of the "atmospheric water tower" over the Tibetan Plateau. Second, we determine the interannual variations in the "atmospheric water tower" reserve. Third, we identify the dominant input or output boundary that drives interannual variations in the reserve. Finally, we explore the forcings that govern interannual variations in the "atmospheric water tower" reserve over the Tibetan Plateau, especially the synergistic effects of climate forcings from three oceans including the North Atlantic, Indian, and Pacific Oceans. Our study provides a vital scientific basis for the water resource management and ecological environment protection in the Tibetan Plateau and surroundings.

2. Material and methods

2.1. The boundaries of the Tibetan Plateau

In order to accurately calculate the reserve of the "atmospheric water tower", we captured the boundary of the entire Tibetan Plateau strictly

along the altitude of 3000 m according to Zhang et al. (2021). The boundary of the Tibetan Plateau is divided into four boundaries (Fig. 1a). *Here*, we define the four boundaries as the eastern, southern, western, and northern boundaries, which are marked by red, sky blue, grass green, and dark green solid lines, respectively (Fig. 1a). Each of the four boundaries includes some zonal sub-boundaries and meridional sub-boundaries (Fig. 1a). Specifically, the eastern boundary includes 5 zonal sub-boundaries (Z1–Z5) and 6 meridional sub-boundaries (M1–M6), the southern boundary includes 8 zonal sub-boundaries (Z6–Z13) and 7 meridional sub-boundaries (M7–M13), the western boundary includes 8 zonal sub-boundaries (Z14–Z21) and 9 meridional sub-boundaries (M14–M22), and the northern boundary includes 14 zonal sub-boundaries (Z22–Z35) and 13 meridional sub-boundaries (M23–M35) (Fig. S1).

2.2. Meteorological data

In this study, the reserve of the "atmospheric water tower" was calculated using the ERA5 monthly averaged data (0.25° × 0.25°, 1000–50 hPa) during the period 1951–2022. The data were provided by the European Centre for Medium-Range Weather Forecasts (ECMWF). The variables include specific humidity (q), U-component of wind (u), V-component of wind (v), and surface pressure (sp). In addition, we also utilized the variables of vertical velocity (w) and geopotential (z) from the ECMWF. In the calculation of the wave activity flux, we used the 200 hPa variables include U-component of wind (u), V-component of wind (v), and geopotential (z) from the ECMWF. We examined the uncertainty of the ERA5 reanalysis data before 1979 due to the sparse satellite observations, and found that the uncertainty does not affect our results (Text S2, Figs. S2). The sea surface temperature (SSTs) data in this study were obtained from HadISST1 with the time resolution and spatial resolution of monthly and 1° × 1°, respectively.

2.3. Calculation of the reserve of the "atmospheric water tower"

We calculated the vertically integrated water vapor flux from the surface to 50 hPa for the period 1951–2022. The vertically integrated water vapor flux (unit: kg m^{-1} s^{-1}) includes the meridional component (Q_φ) and the zonal component (Q_λ), which can be calculated as follows (Sun et al., 2011; Trenberth, 1991):

$$Q_\varphi = -\frac{1}{g}\int_{P_s}^{P_t}(qv)dp \tag{1}$$

$$Q_\lambda = -\frac{1}{g}\int_{P_s}^{P_t}(qu)dp \tag{2}$$

where g represents the gravity acceleration (= 9.80665 m s^{-2}); p_s represents the surface pressure (Pa), p_t represents the top pressure (50 hPa); q represents the specific humidity (kg kg^{-1}); v and u represent the northward and eastward components of the wind (m s^{-1}), respectively.

The water vapor fluxes across each of the zonal (Q_Z) and meridional (Q_M) sub-boundaries can be calculated using Eqs. (3)–4) as follows:

$$Q_Z = \int_{\lambda_W}^{\lambda_E} Q_\varphi a\cos\varphi d\lambda \tag{3}$$

$$Q_M = \int_{\varphi_S}^{\varphi_N} Q_\lambda a\, d\varphi \tag{4}$$

where λ_W denotes the longitude of the westernmost point of the zonal boundary, λ_E denotes the longitude of the easternmost point of the zonal boundary, φ_S denotes the latitude of the southernmost point of the meridional boundary, φ_N denotes the latitude of the northernmost point of the meridional boundary, and a is the Earth's radius (6.37 × 10^6 m).

The water vapor fluxes across the eastern (Q_E), southern (Q_S), western (Q_W), and northern (Q_N) boundaries can be calculated as follows:

$$Q_E = \sum_1^n Q_Z + \sum_1^n Q_M \tag{5}$$

$$Q_S = \sum_1^n Q_Z + \sum_1^n Q_M \tag{6}$$

$$Q_W = \sum_1^n Q_Z + \sum_1^n Q_M \tag{7}$$

$$Q_N = \sum_1^n Q_Z + \sum_1^n Q_M \tag{8}$$

The reserve of the "atmospheric water tower" can be calculated: $Q = Q_E + Q_S + Q_W + Q_N$.

The detailed calculation method can be found in Supporting Text S1.

2.4. Related climate indices

In order to analyze the relationships between the reserve of the "atmospheric water tower" over the Tibetan Plateau and climate forcings from three oceans, in this study we applied key climate indices including the Atlantic Multidecadal Oscillation Index (AMO), Indian Ocean Basin-Wide Index (IOBW), Southern Oscillation Index (SOI), and Niño 3.4. The AMO is a coherent pattern of variability in basin-wide North Atlantic SSTs, and the AMO index was obtained from National Oceanic and Atmospheric Administration/National Centers for Environmental Information (NOAA/NCEI) based on the NOAA ERSSTV5 (https://www.psl.noaa.gov/data/timeseries/AMO/). The IOBW is represented as the area-averaged sea surface temperature (SST) anomaly in the tropical Indian Ocean (20°S–20°N, 40°–110°E), and the IOBW index was provided by National Climate Centre (https://cmdp.ncc-cma.net/Monitoring/cn_index_130.php). The SOI is defined as the normalized pressure difference between Tahiti and Darwin based on the method given by Ropelewski and Jones (1987), and the SOI time series was obtained from the National Oceanic and Atmospheric Administration (NOAA) (https://psl.noaa.gov/data/correlation/soi.data). The positive SOI values indicate La Niña episodes, while the negative SOI values indicate El Niño episodes. The Niño 3.4 is the area averaged anomalies over the Niño 3.4 region (5°N–5°S, 170°–120°W) using a climatology of 1981–2010. The Niño 3.4 index was obtained from https://psl.noaa.gov/data/timeseries/month/data/nino34.long.anom.data. To demonstrate the climatic transition around 1973, we utilized the Pacific Decadal Oscillation (PDO) index (https://psl.noaa.gov/gcos_wgsp/Timeseries/PDO/).

2.5. Wave activity flux

To explore the impacts of the climate forcing from the North Atlantic Ocean on the interannual variations in the reserve of "atmospheric water tower" over the Tibetan Plateau, a two-dimensional Takaya–Nakamura approach (Takaya and Nakamura, 2001) was used in this study. The Takaya–Nakamura wave activity flux enhances the meridional component, providing a more accurate description of large-amplitude Rossby long-wave disturbances in zonally non-uniform flow (Takaya and Nakamura, 2001). The two-dimensional Takaya–Nakamura approach can be calculated as follows (Takaya and Nakamura, 2001; Liu et al., 2023):

$$W = \frac{P}{2|U|}\begin{pmatrix} \overline{u}(\psi_x'^2 - \psi'\psi'_{xx}) + \overline{v}(\psi'_x\psi'_y - \psi'\psi'_{xy}) \\ \overline{u}(\psi'_x\psi'_y - \psi'\psi'_{xy}) + \overline{v}(\psi_y'^2 - \psi'\psi'_{yy}) \end{pmatrix} \tag{9}$$

where W denotes wave activity flux; P denotes pressure layers; $U = (u, v)$ denotes horizontal winds, the u and v denote the U-component of wind and V-component of wind, respectively; ψ denotes stream function, $\psi = \Phi/f$, Φ is the geopotential, and f is the Coriolis parameter ($f = 2\Omega\sin\varphi$, Ω is the earth's rotation rate). Overbars and primes denote the climatology

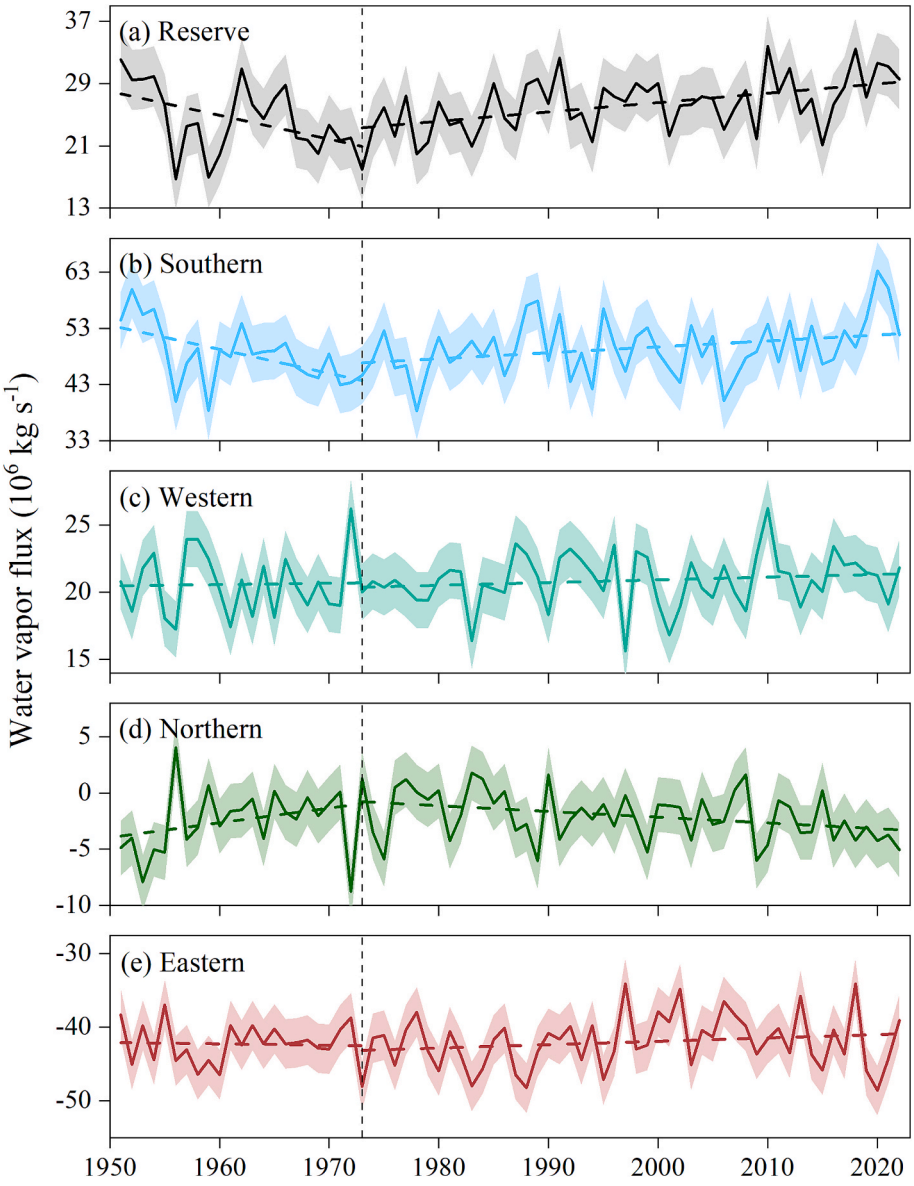

Fig. 2. Interannual variations in the "atmospheric water tower" reserve over the Tibetan Plateau (a) and water vapor fluxes across the southern (b), western (c), northern (d), and eastern (e) boundaries over 1951–2022. The vertical dashed lines indicate the shift of the interannual variations in the reserve in 1973. The negative values indicate that water vapor flows out from the Tibetan Plateau. The larger the absolute value of the negative value, the more water vapor flows out of the Tibetan Plateau.

mean and monthly disturbances, respectively.

3. Results

3.1. Climatological mean reserve of the "atmospheric water tower"

We calculated the climatological mean water vapor flux across each boundary of the Tibetan Plateau over 1951–2022 (Fig. 1b). The water vapor fluxes across the southern, western, northern, and eastern boundaries are 49.17 × 10^6 kg s^{-1}, 20.80 × 10^6 kg s^{-1}, −2.19 × 10^6 kg s^{-1}, and −42.02 × 10^6 kg s^{-1}, respectively. The positive and negative values indicate input and output water vapor, respectively. Thus, the water vapor flows into the Tibetan Plateau across the southern and western boundaries and flows out across the eastern and northern boundaries (Fig. 1b). Our determinations of the boundaries are consistent with the results of Feng and Zhou (2012), Yan et al. (2020) and Li et al. (2022b). However, other studies such as Xu et al. (2020) suggested that the water vapor flows into the Tibetan Plateau across the southern, western, and northern boundaries, while it flows out across the eastern boundary. It should be noted that the northern boundary of Xu et al. (2020) is located within the inner Tibetan Plateau, which allows it to readily capture more water vapor input by the westerlies and thus is simply identified as a water vapor input boundary with a straight line (Fig. S3). Since the identification of input or output water vapor is highly sensitive to the location of the chosen boundary, we strictly constructed the northern boundary with 27 sub-boundaries (Fig. S3). Our northern boundary is considerably longer and exhibits an "output–input–output" water vapor transport pattern (Fig. S3). Moreover, we found that the output water vapor across the northern boundary is larger than the input water vapor across the northern boundary (Fig. 1b, Fig. S3). Hence, the northern boundary is a net output boundary. Indeed, a high-precision boundary is essential for accurately constraining the "atmospheric water tower" reserve over the Tibetan Plateau.

Based on the water vapor fluxes across the four boundaries mentioned above, we calculated the climatological mean reserve of the "atmospheric water tower" over the Tibetan Plateau as (25.76 ± 3.83)

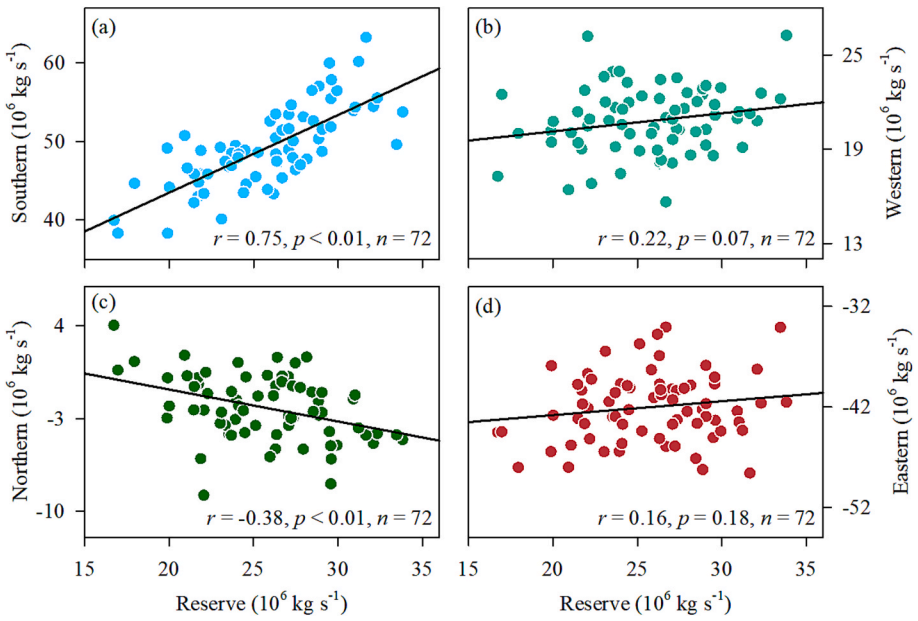

Fig. 3. Correlations between the interannual variations of the "atmospheric water tower" reserve over the Tibetan Plateau and the corresponding water vapor flux across the southern (a), western (b), northern (c), and eastern (d) boundaries over 1951–2022.

$\times 10^6$ kg s^{-1}. Our result differs from previous studies: the climatological mean reserve of the "atmospheric water tower" was calculated by Yan et al. (2020) and Xu et al. (2020) as 1046 Gt yr^{-1} (=33.17 $\times 10^6$ kg s^{-1}) and 11.85 $\times 10^6$ kg s^{-1}, respectively (Table S1 and S2). As mentioned above, the boundary of the entire Tibetan Plateau used in our study was strictly defined along the altitude of 3000 m, which is notably different from the other studies. Hence, we propose that the difference in the boundaries is one of the main factors that affect the calculations for the reserve of the "atmospheric water tower." To verify our conjecture, we replicated some studies using their respective boundaries and found that the calculated reserves indeed exhibited substantial divergence. We also compared two previous studies that used similar boundaries but utilized reanalysis data with different spatial resolutions (Li et al., 2022b; Yu et al., 2022), and found that the calculated reserve based on the high spatial resolution ERA5 data (0.25° × 0.25°) (Li et al., 2022b) differed significantly from that using the lower spatial resolution ERA5 data (2.5° × 2.5°) (Yu et al., 2022) (Table S2). These results demonstrate that the considerable discrepancies in the estimated reserve are primarily related to the different boundaries of the Tibetan Plateau and data with different spatial resolutions. Clearly, the better constrained boundary design and high-resolution data employed in our calculation have been essential for a robust evaluation of the "atmospheric water tower" reserve over the Tibetan Plateau.

One might argue that different study periods and different integration ranges could also significantly influence the calculated results of the "atmospheric water tower" reserve. To test this contention, we calculated the climatological mean reserve of "atmospheric water tower" for different study periods and with different integration ranges based on the boundary defined in our study. The results demonstrate that there are very small differences in the calculated reserves across different study periods and integration ranges (Table S3).

3.2. *Interannual variations in the "atmospheric water tower" reserve*

The interannual variations in the reserve of the "atmospheric water tower" over the Tibetan Plateau from 1951 to 2022 are shown in Fig. 2. The results show that the "atmospheric water tower" reserve exhibits a significant and decreasing trend from 1951 to 1973, and a significant and increasing trend from 1974 to 2022 (Fig. 2a), with slopes of −0.31 $\times 10^6$ kg s^{-1} yr^{-1} ($p < 0.05$) and 0.11 $\times 10^6$ kg s^{-1} yr^{-1} ($p < 0.01$), respectively. Similarly, a decreasing and increasing trend in the water vapor flux is evident across the southern boundary over 1951–1973 and 1974–2022, respectively (Fig. 2b). The linear trends of interannual variations in the water vapor flux across the southern boundary over 1951–1973 and 1974–2022 are −0.43 $\times 10^6$ kg s^{-1} yr^{-1} ($p < 0.01$) and 0.10 $\times 10^6$ kg s^{-1} yr^{-1} ($p < 0.05$), respectively. Moreover, interannual variations in the water vapor flux across the southern boundary and the "atmospheric water tower" reserve show a strongly positive and significant correlation ($r = 0.75$, $p < 0.01$, $n = 72$) (Fig. 3a). Therefore, the southern boundary makes an important contribution to the increase of the "atmospheric water tower.".

In comparison, the trends of the interannual variations of the water vapor flux across the western boundary over 1951–1973 and 1974–2022 are not significant (0.01 $\times 10^6$ kg s^{-1} yr^{-1} and 0.02 $\times 10^6$ kg s^{-1} yr^{-1}, respectively) (Fig. 2c, Table S4), although the western boundary is an input boundary with a large water vapor flux (20.80 $\times 10^6$ kg s^{-1}). That is, both in 1951–1973 and in 1974–2022, the increasing trend of the water vapor flux across the western boundary was very weak. Moreover, the water vapor flux across the western boundary shows a relatively weak correlation with the "atmospheric water tower" reserve ($r = 0.22$, $p = 0.07$) (Fig. 3b). The weak increasing trend and correlation indicate a relatively limited influence of the water vapor flux across the western boundary on the trend of interannual variations in the "atmospheric water tower" reserve from 1951 to 2022.

Similarly, the trend of interannual variations in water vapor flux across the northern boundary over 1951–1973 is also not significant, but it does exhibit a significant and decreasing trend over 1974–2022, with a slope of −0.05 $\times 10^6$ kg s^{-1} yr^{-1} ($p < 0.05$) (Fig. 2d). The water vapor flux across the northern boundary is significant and negatively correlated with the "atmospheric water tower" reserve over 1951–2022 ($r = -0.38$, $p < 0.01$, $n = 72$) (Fig. 3c). Clearly, the northern boundary is the major water vapor output boundary. Hence, the water vapor flux across the northern boundary negatively impacts the reserve of the "atmospheric water tower.".

The trends of the interannual variations of the output water vapor across the eastern boundary over 1951–1973 and 1974–2022 are also not significant (Fig. 2e), and there is no relationship between interannual variations in water vapor flux across the eastern boundary and the "atmospheric water tower" reserve over the Tibetan Plateau (Fig. 3d). Thus, the contribution of the water vapor flux across the eastern

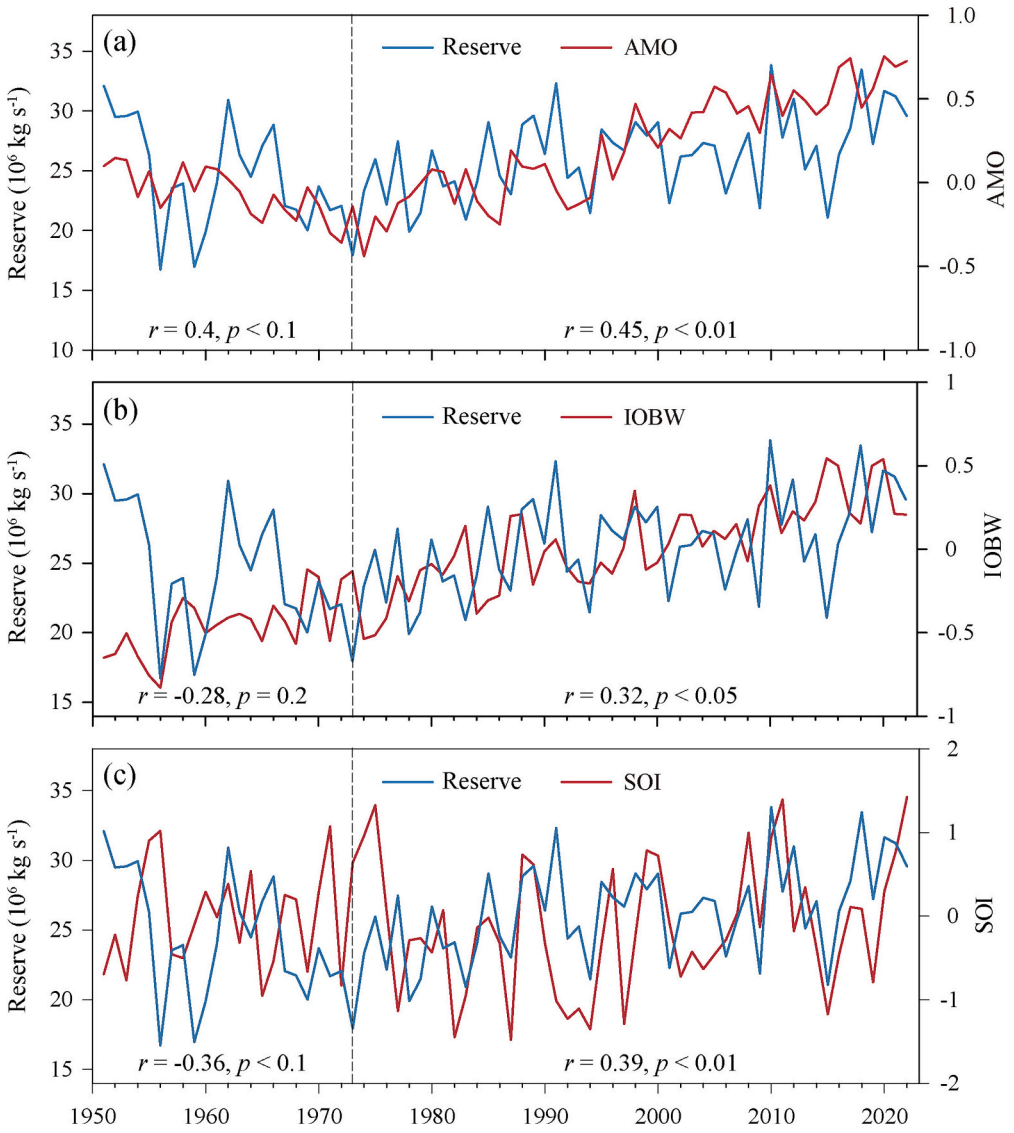

Fig. 4. Interannual variations of the "atmospheric water tower" reserve and the corresponding AMO (a), IOBW (b), and SOI (c).

boundary to the trend of the "atmospheric water tower" is very weak.

Based on the trends of the interannual variations in water vapor flux across the four boundaries and their correlations with the "atmospheric water tower" reserve over the Tibetan Plateau, we find that the increasing trend in the reserve is primarily driven by the significant increase in input water vapor flux across the southern boundary.

3.3. Relationships between the reserve and climate forcings from the three oceans

The variations in the North Atlantic Ocean are commonly linked to the water vapor transport to the Tibetan Plateau, thus affecting the terrestrial water storage across the region (Zhang et al., 2023). The relationships between the interannual variations in the "atmospheric water tower" reserve over the Tibetan Plateau and the corresponding AMO are shown in Fig. 4a. The result shows that the reserve and the AMO index follow the same fluctuation patterns from 1951 to 2022. That is, similar to the reserve, the corresponding AMO index decreased gradually from 1951 to 1973, but increased gradually from 1974 to 2022 (here we defined the periods 1951–1973 and 1974–2022 as Periods I and II, respectively). Our results show that the interannual variations in the reserve have a weak-to-moderate positive correlation with the corresponding AMO index during Period I ($r = 0.4, p < 0.1$), whereas it exhibits a significant positive correlation during Period II ($r = 0.45, p < 0.01$) (Fig. 4a). Clearly, both the interannual variations in the reserve and the AMO shifted around 1973. The result implies that the shift of interannual variation in the reserve is linked to a major shift of the AMO which occurred around 1973. Hence, we propose that the weakening AMO before 1973 drove the decrease in the "atmospheric water tower" reserve while the strengthening AMO after 1973 led to the gradual increase in the "atmospheric water tower" reserve.

The Indian Ocean sea surface temperatures (SSTs) also play a crucial role in influencing water vapor transported to the Tibetan Plateau (Chen et al., 2022b). The warmer Indian Ocean SSTs will cause the strengthening IOBW (Yang et al., 2009; Chen and You, 2017; Chen et al., 2022b; Wei and Yu, 2024). Hence, the IOBW index reflects variations in Indian Ocean SSTs. The relationship between the IOBW and the "atmospheric water tower" reserve over the Tibetan Plateau is shown in Fig. 4b. We found that there was no significant correlation between the reserve and IOBW over 1951–1973 ($r = -0.28, p = 0.2$) (Fig. 4b). This result indicates that the IOBW has limited impact on the reserve during Period I. However, the reserve and IOBW display a significant and positive correlation over 1974–2022 ($r = 0.32, p < 0.05$) (Fig. 4b). This indicates that the reserve of "atmospheric water tower" can be influenced by the

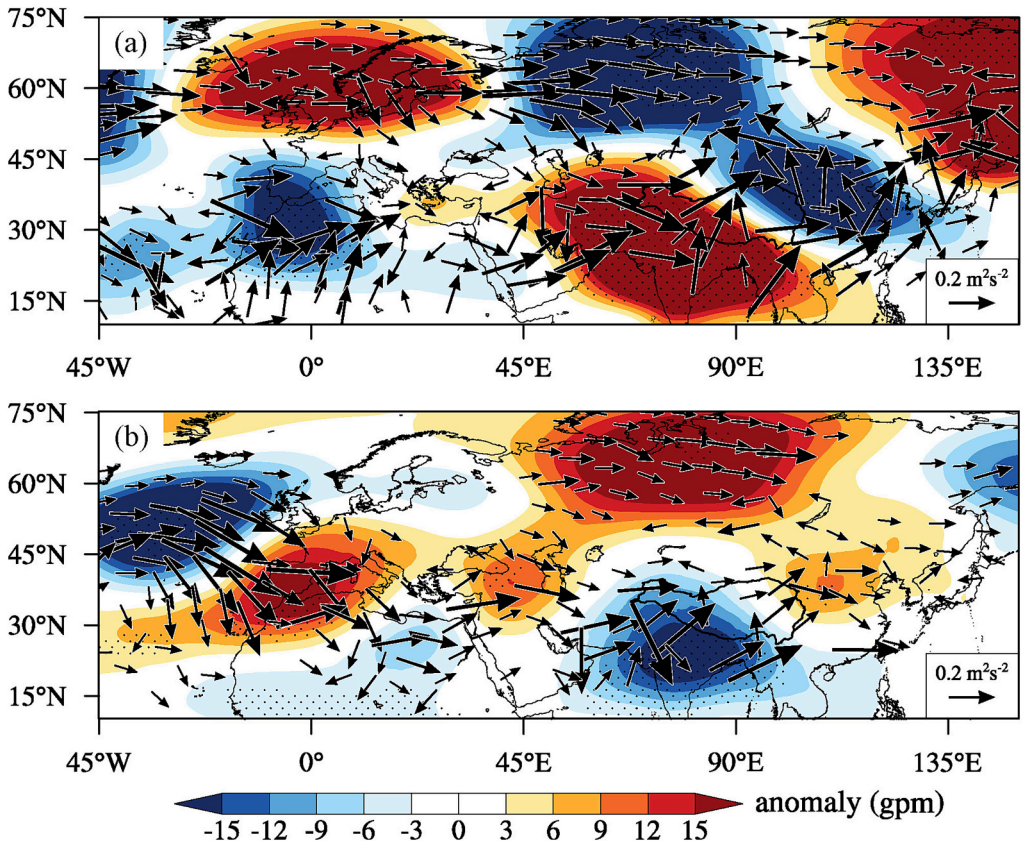

Fig. 5. (a) The differences of wave activity flux (vector) and geopotential heights (shading) at 200 hPa between 1971–1975 and 1951–1955. (b) Same as (a), but for the differences between 2018–2022 and 1971–1975. The black dots denote differences that are significant at the 90% confidence level.

Indian Ocean SSTs after 1973.

We also investigated the relationship between the "atmospheric water tower" reserve and El Niño-Southern Oscillation (ENSO) (Fig. 4c). The result indicates that the "atmospheric water tower" reserve was significantly and positively correlated with the SOI during Period II (1974–2022) ($r = 0.39$, $p < 0.01$) (Fig. 4c), although the reserve was weakly and negatively correlated with the SOI during Period I (1951–1973) ($r = -0.36$, $p < 0.1$) (Fig. 4c). In addition, the reserve shows a weak positive correlation with the Niño 3.4 during Period I ($r = 0.14$, $p = 0.53$), whereas it exhibits a significant negative correlation with the Nino 3.4 during Period II ($r = -0.32$, $p < 0.05$) (Fig. S4). Consequently, we propose that the Pacific Ocean has a stronger influence on the reserve of "atmospheric water tower" over the Tibetan Plateau during Period II than during Period I.

4. Discussion

4.1. The "atmospheric water tower" reserve and AMO

The wave activity flux is relevant to "atmospheric water tower" dynamics, as it transmits the climatic signals of the North Atlantic Ocean to the Tibetan Plateau. The Rossby wave activity flux can be employed to analyze how atmospheric circulation anomalies upstream of the Tibetan Plateau influence local upper-tropospheric geopotential height anomalies. The variation in North Atlantic SSTs triggers wave trains and energy that propagates toward downstream regions, which then modulates atmospheric circulation anomalies over the Tibetan Plateau and ultimately plays a critical role in the region's water vapor transport and atmospheric circulation changes (Wang et al., 2017; Gao et al., 2021; Wang et al., 2021). Obviously, through the Rossby wave activity, the climate forcing of the North Atlantic Ocean can significantly influence variations in the "atmospheric water tower" reserve over the Tibetan Plateau. To investigate how the climate forcing from the North Atlantic Ocean affect the reserve, we examined the anomalies in wave activity flux propagation and the atmospheric circulation patterns over 1951–1955, 1971–1975, and 2018–2022, based on the patterns of the reserve of the "atmospheric water tower" and the AMO. That is, the reserve and the AMO both showed relatively high values over 1951–1955 and over 2018–2022, but both showed relatively low values over 1971–1975 (around 1973). First, we calculated the differences of wave activity flux (vector) and the geopotential heights (shading) at 200 hPa between 1971–1975 and 1951–1955 (Fig. 5a). It can be found that two dominant wave trains propagated across the Eurasian Continent, both originating from the North Atlantic. These wave trains induced alternative cyclonic and anticyclonic anomalies over the subtropical and mid-high latitude westerly jet regions, respectively. Consequently, an anomalous cyclone occurred over North China and an anomalous anticyclone appeared over India. The synergistic interaction between the northwesterlies along the northern flank of the anticyclone and the northwesterlies along the southern flank of the cyclone suppresses moisture advection toward the southern Tibetan Plateau, causing a decline in the "atmospheric water tower" reserve over the Tibetan Plateau during the period 1951–1973.

We then conducted analysis on the differences in wave activity flux (vector) and the geopotential heights (shading) at 200 hPa between 2018–2022 and 1971–1975 (Fig. 5b). The result showed that the wave activity flux emanated from the North Atlantic, then travelled through Southwestern Europe, and continued to propagate eastward through Western Asia, and finally induced the anomalous cyclonic circulation over India (Fig. 5b). In addition, an anomalous anticyclonic circulation appeared over North China. Consequently, anomalous southwesterlies along the southern flank of the cyclone and southeasterlies along the southern flank of the anticyclone facilitated moisture advection from the northern Indian Ocean and Pacific Ocean toward the Tibetan Plateau,

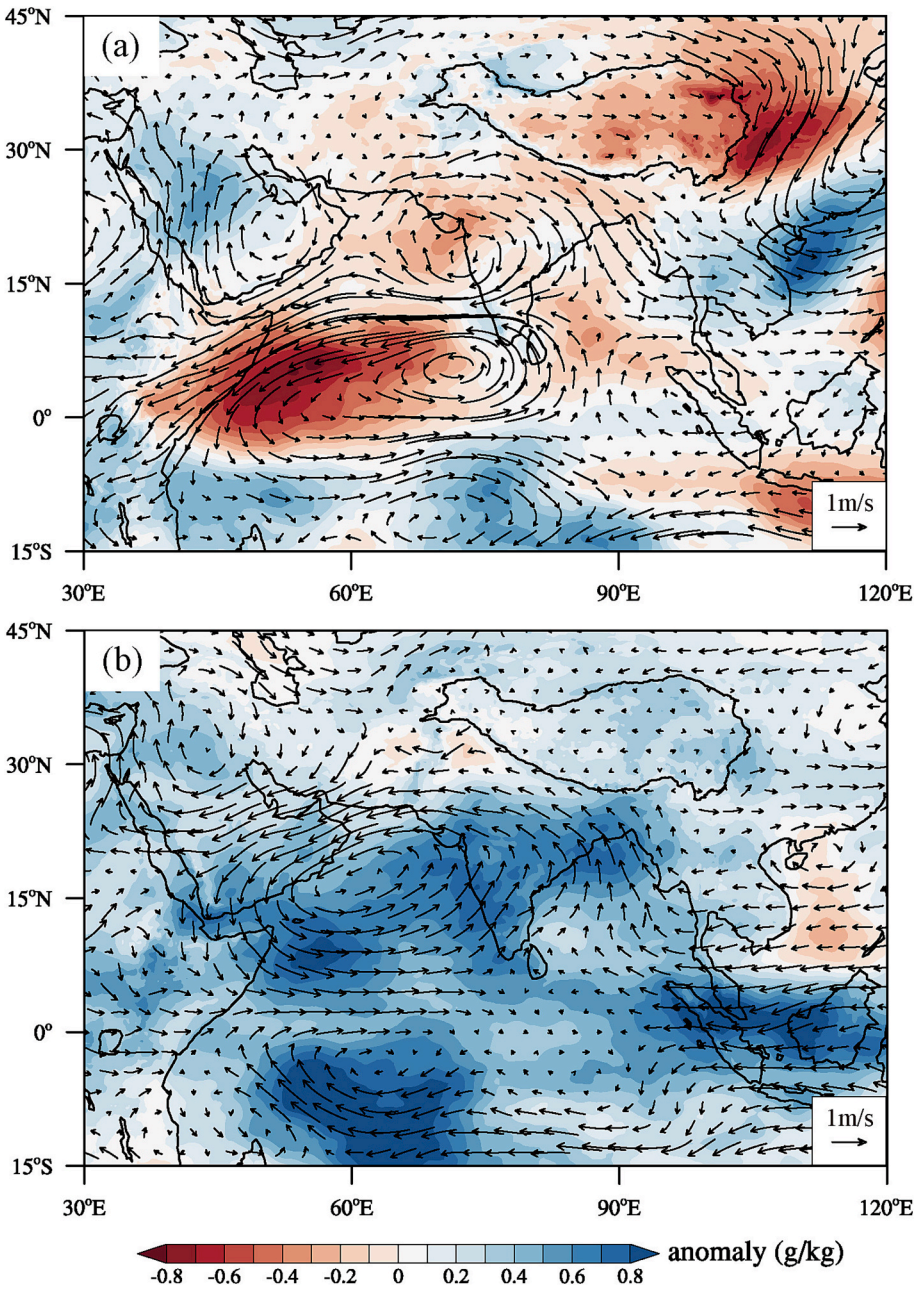

Fig. 6. (a) The differences of wind (vector) and specific humidity (shading) fields at 700 hPa between the strong IOBW (1969, 1970, 1972, and 1973) and the weak IOBW (1951, 1954, 1955, and 1956) over 1951–1973. (b) Same as (a), but for the differences between the strong IOBW (2010, 2015, 2016, 2019, and 2020) and the weak IOBW (1974, 1975, 1976, 1978, and 1984) over 1974–2022.

resulting in a significant increase in the "atmospheric water tower" reserve over the Tibetan Plateau from 1974 to 2022.

4.2. *The "atmospheric water tower" reserve and IOBW*

To investigate how the climate forcing from the Indian Ocean influences the reserve, we identified and analyzed the strong and weak IOBW years. We first calculated the mean and standard deviation (1σ) of the IOBW index for Period I and Period II, respectively. We then classified the years with an index value exceeding and below the mean ± 1σ into strong and weak IOBW years. To ensure a fair comparison, we selected an equal number of strong and weak years. Specifically, for Period I, we identified 1969, 1970, 1972, and 1973 as the strong IOBW years, and identified 1951, 1954, 1955, and 1956 as the weak IOBW years. For Period II, we identified 2010, 2015, 2016, 2019, and 2020 as the strong IOBW years, and identified 1974, 1975, 1976, 1978, and 1984 as the weak IOBW years (Fig. S5). Finally, we calculated the differences of wind and specific humidity fields at 700 hPa between the strong IOBW (1969, 1970, 1972, and 1973) and the weak IOBW (1951, 1954, 1955, and 1956) during Period I (Fig. 6a). The results indicate that the water vapor flowed out the Tibetan Plateau. Therefore, the "atmospheric water tower" reserve over the Tibetan Plateau decreased during Period I and has little correlation with the Indian Ocean SSTs.

We then calculated the differences of wind and specific humidity fields at 700 hPa between the strong IOBW (2010, 2015, 2016, 2019, and 2020) and the weak IOBW (1974, 1975, 1976, 1978, and 1984) during Period II. It can be seen that over this period the anomalous cyclone over the Arabian Sea drives large amounts of water vapor to the Bay of Bengal. Then, the water vapor flows into the Tibetan Plateau along a channel on the eastern section of the cyclone and results in an

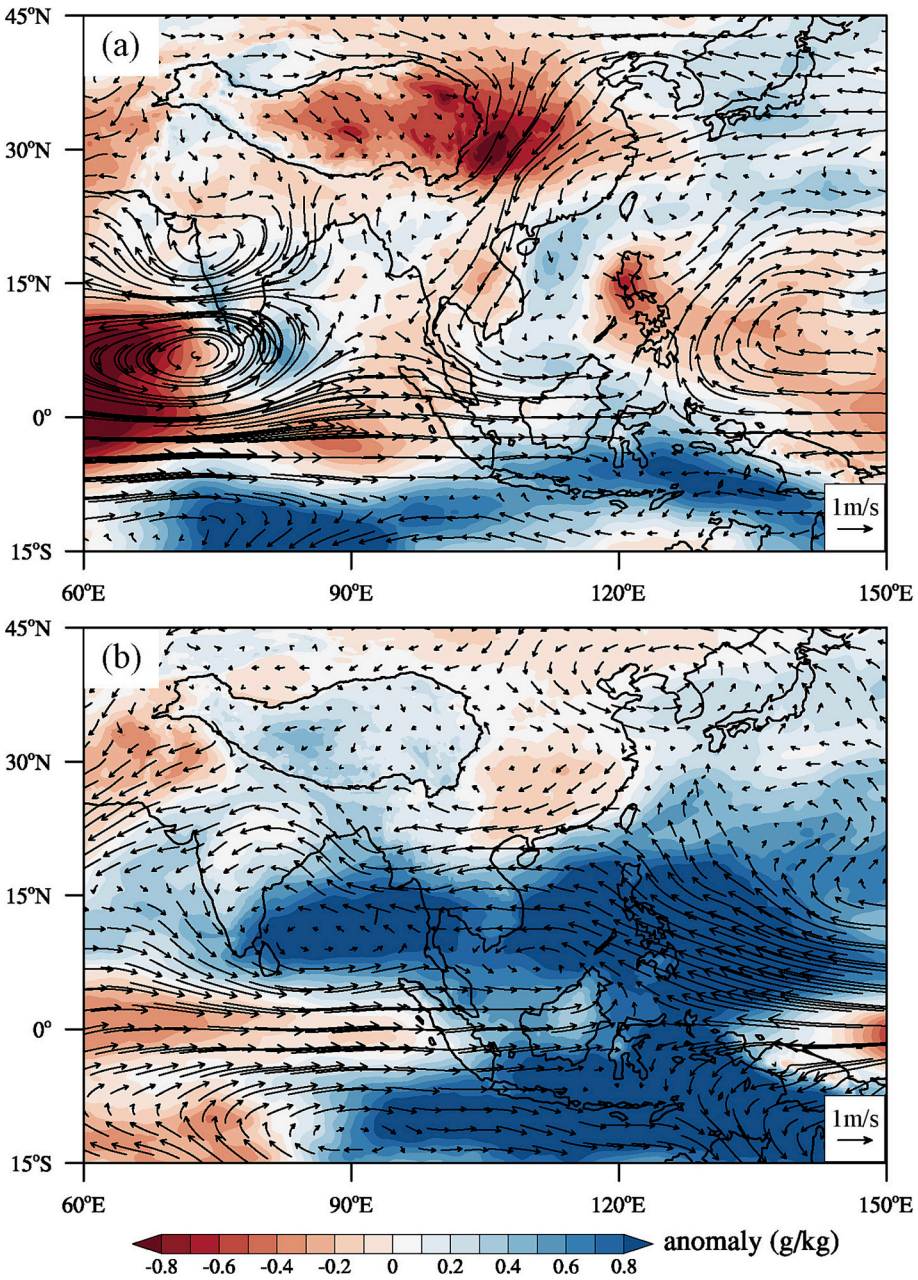

Fig. 7. (a) The differences of wind (vector) and specific humidity (shading) fields at 700 hPa between the positive SOI (La Niña episodes, 1967, 1970, 1971, and 1973) and the negative SOI (El Niño episodes, 1951, 1952, 1953, and 1957) over 1951–1973. (b) Same as (a), but for the differences between the positive SOI (La Niña episodes, 2000, 2008, 2010, 2011, and 2022) and the negative SOI (El Niño episodes, 1977, 1982, 1987, 1992, and 1994) over 1974–2022.

increasing trend in the "atmospheric water tower" reserve (Fig. 6b). Moreover, the specific humidity in the Tibetan Plateau during Period II was more humid than that during Period I (Fig. 6). Hence, our findings demonstrate that the Indian Ocean SSTs play an important role to drive the increasing trend in the "atmospheric water tower" reserve over 1974–2022.

4.3. The "atmospheric water tower" reserve and ENSO

To investigate the climate forcing from the Pacific Ocean on the reserve, we analyzed the water vapor transport associated with ENSO. During Period I, the specific humidity in the Tibetan Plateau displays a negative anomaly between the positive SOI (La Niña episodes, 1967, 1970, 1971, and 1973) and the negative SOI (El Niño episodes, 1951, 1952, 1953, and 1957) over 1951–1973 (Fig. 7a). Moreover, relatively more water vapor flowed out of the Tibetan Plateau compared to Period II. Therefore, during Period I, the water vapor from the Pacific Ocean did not affect the "atmospheric water tower" reserve. That is why there was no relationship between the increase in the "atmospheric water tower" reserve and the SOI.

During Period II, the specific humidity in the Tibetan Plateau displays a positive anomaly between the positive SOI (La Niña episodes, 2000, 2008, 2010, 2011, and 2022) and the negative SOI (El Niño episodes, 1977, 1982, 1987, 1992, and 1994) over 1974–2022. Furthermore, the convergence of considerable water vapor over the Western Pacific Ocean was transported from east to west (Fig. 7b). As a result, a clear water vapor channel forms in the Western Pacific Ocean (Fig. 7b). In addition, an anomalous cyclone occurs in the South China Sea, which carries water vapor from the Western Pacific Ocean to the Bay of Bengal. The water vapor is then transported along the channel and into the

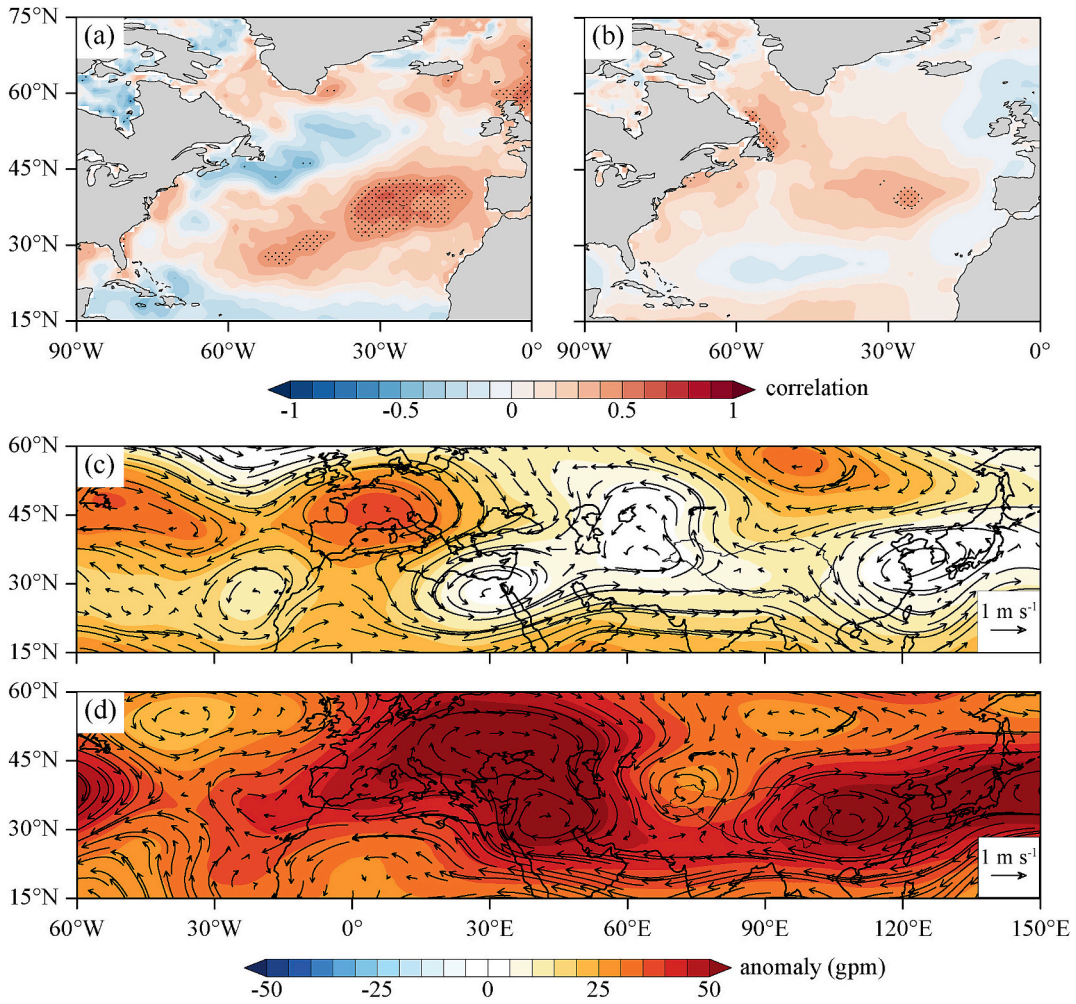

Fig. 8. (a) Correlation between the "atmospheric water tower" reserve and North Atlantic sea surface temperatures (SSTs) during 1974–1994. (b) Same as (a), but for 1995–2022. (c) The differences of geopotential heights (shading) and wind fields (vector) at 200 hPa between 1992–1996 and 1974–1978. (d) Same as (c), but for the differences between 2018–2022 and 1992–1996. The black dots denote differences that are significant at the 95% confidence level in (a), (b).

Tibetan Plateau (Fig. 7b). Hence, more water vapor is transported westward from the Western Pacific Ocean to the Tibetan Plateau via the South China Sea and the Bay of Bengal. This finding indicates that La Niña episodes (the positive SOI values) causes an increasing trend in the "atmospheric water tower" reserve over the Tibetan Plateau during Period II (Fig. 7b), similar to the findings from previous research (Jing et al., 2021).

4.4. Synergistic effects of climate forcings from three oceans on the reserve

Based on the analysis above, only the interannual variation in the AMO is consistent with the pattern of the "atmospheric water tower" reserve over the entire period (1951–2022). Hence, the AMO plays a dominant role controlling the interannual variation in the "atmospheric water tower" reserve. We note that during Period I, the correlation between the SOI and the "atmospheric water tower" reserve ($r = -0.36$, $p < 0.1$) (Fig. 4c) is comparable in magnitude to that between the AMO and the reserve ($r = 0.4$, $p < 0.1$) (Fig. 4a). However, if ENSO were a key driver in Period I, the SOI should exhibit a positive correlation with the reserve, as is the case in Period II (Fig. 4c). The observed negative correlation during Period I, therefore, does not support this expectation. This finding indicates that ENSO has no contribution to the variation in the reserve during Period I. Similarly, IOBW is negatively correlated with the reserve; as a consequence, its contribution to the variation in the reserve is also negligible during Period I (Fig. 4b). In contrast, during Period II (1974–2022), both IOBW and SOI show significant positive correlations with the reserve ($r = 0.32$, $p < 0.05$ and $r = 0.39$, $p < 0.01$, respectively; Fig. 4b and Fig. 4c), indicating that their contributions to the reserve are considerable.

We now provide additional evidence to confirm why the AMO's influence is considered dominant from the perspective of the circulation patterns. As mentioned above, the combined impact of the cyclone over North China and anticyclone over India suppressed the water vapor from the Pacific Ocean to transport into the Tibetan Plateau during Period I (Fig. 5a). Moreover, the differences of wind and specific humidity fields at 700 hPa between the strong IOBW and the weak IOBW (Fig. 6a) or between the positive SOI and the negative SOI (Fig. 7a) both show that the water vapor always flowed out of the Tibetan Plateau during Period I. In fact, during Period I, the circulation patterns for both IOBW (Fig. 6a) and SOI (Fig. 7a) were highly similar to that for AMO (Fig. 5a), as manifested by the anomalous anticyclone over India, indicating that AMO played a strongly dominant role during this period. Consequently, the gradually weakening AMO during Period I (1951–1973) led to the remarkable decline of the "atmospheric water tower" reserve over the Tibetan Plateau. The strong influence of the AMO masks the roles of climate forcings from the Indian and Pacific Oceans in the interannual variation of the "atmospheric water tower" reserve during Period I.

During Period II (1974–2022), however, the roles of climate forcings (IOBW and ENSO) from the Indian and Pacific Oceans on the interannual

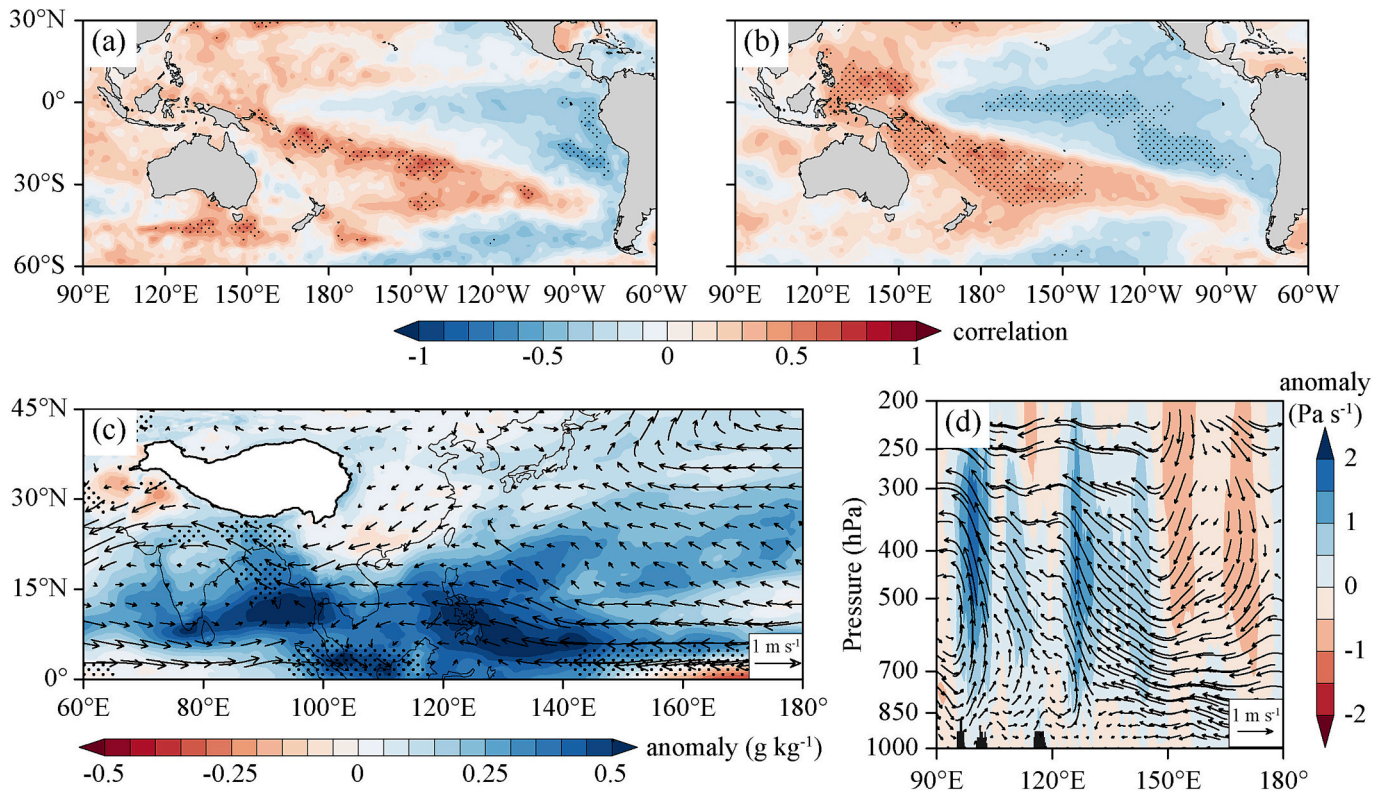

Fig. 9. (a) Correlation between the "atmospheric water tower" reserve and Pacific sea surface temperatures (SSTs) during 1974–1994. (b) Same as (a), but for 1995–2022. (c) The differences of specific humidity (shading) and wind fields (vector) at 700 hPa between 1995–2022 and 1974–1994. (d) Cross section of the difference of the vertical velocity (shading) and wind fields (vector) averaged from 0° to 10°N between 1995–2022 and 1974–1994. The black dots denote differences that are significant at the 95% confidence level in (a), (b) and (c).

variation in the "atmospheric water tower" reserve have enhanced. That is, synergistic effects of climate forcings (including AMO, IOBW, and ENSO) from three oceans transported more water vapor to the Tibetan Plateau and contributed to the significant increasing trend of the "atmospheric water tower" reserve.

We also found that during the last 28 years (1995–2022), the positive correlation between the "atmospheric water tower" reserve and the AMO has weakened significantly (r = 0.34, p = 0.07), although the positive correlation between the reserve and the AMO remained throughout the entire period. This means that the influence of the AMO on the "atmospheric water tower" reserve is not constant. Instead, its impact on the reserve has gradually weakened over time. In comparison, the correlation between the "atmospheric water tower" reserve and the SOI index has changed from a weak and negative correlation (r = -0.36, p = 0.09 for the period 1951–1973) to a weak positive correlation (r = 0.18, p = 0.43 for the period 1974–1994) and then to a significant positive correlation (r = 0.46, $p < 0.05$ for the period 1995–2022) over time. This finding suggests that the dominant forcings driving the reserve's increasing trend has transitioned eastward from the North Atlantic Ocean to the Pacific Ocean.

To investigate the mechanisms behind the transition of the North Atlantic's influence on the "atmospheric water tower" reserve over the Tibetan Plateau—which transitioned from strong to weak around 1994—we analyzed the correlations between the "atmospheric water tower" reserve and North Atlantic SSTs (Fig. 8). Additionally, we examined geopotential heights and wind fields for the two periods of 1974–1994 and 1995–2022 (Fig. 8). The results indicate that during 1974–1994, the "atmospheric water tower" reserve showed a significant positive correlation with North Atlantic SSTs (Fig. 8a). However, during 1995–2022, the positive correlations weakened substantially, with the significant correlation area shrinking to the central North Atlantic Ocean (Fig. 8b). To further investigate the mechanisms behind this transition, we selected three critical 5-year phases including the initial phase (1974–1978), the transition phase (1992–1996, centered on 1994), and the recent phase (2018–2022) and calculated the differences of the geopotential heights and wind fields at 200 hPa between 1992–1996 and 1974–1978, as well as between 2018–2022 and 1992–1996 (Fig. 8c, d). The results show that a cyclonic anomaly circulation appeared over East Asia before 1994, accompanied by strong westerly anomalies in the subtropical region, causing more water vapor transport from the North Atlantic Ocean to the Tibetan Plateau (Fig. 8c). In comparison, after 1994 an anticyclonic anomaly emerged over East Asia, and the subtropical westerlies weakened significantly, reducing water vapor transport from the North Atlantic Ocean to the Tibetan Plateau. The anomalies in the 500 hPa geopotential height and wind fields also confirmed this opposing water vapor transport pattern (Fig. S6). The findings demonstrate that the influence of the AMO on the "atmospheric water tower" reserve weakened significantly after 1994. This weakening led to changes in the dominant water vapor sources and factors governing the "atmospheric water tower" reserve over the Tibetan Plateau.

In contrast, the Pacific's influence gradually strengthened after 1994. Compared to 1974–1994, the correlations between the "atmospheric water tower" reserve over the Tibetan Plateau and Pacific SSTs intensified significantly during 1995–2022, accompanied by a substantial expansion of the statistically significant correlation area. Notably, the area of significant positive correlation extended from the South Pacific to the northwestern Pacific. This drove pronounced easterly anomalies to emerge in the northern equatorial Pacific (0–10°N) during 1995–2022 (Fig. 9c and Fig. S7). This significantly enhancing westward water vapor was transported from the Pacific and flowed into the Tibetan Plateau across its southern boundary. Additionally, the equatorial easterly anomalies from the surface to 400 hPa were observed east of 120°E in the northern equatorial region (Fig. 9d), further facilitating westward water vapor transport from the Pacific. Clearly, the enhancing

westward transport of Pacific water vapor has compensated for the reduced Atlantic water vapor transport during 1995–2022. Consequently, the "atmospheric water tower" reserve over the Tibetan Plateau maintained its increasing trend from 1995 to 2022.

5. Conclusions

This study determined the reserve of the "atmospheric water tower" over the Tibetan Plateau from 1951 to 2022 and the associated mechanisms that influence its interannual trends. The results indicate that the climatological mean reserve of the "atmospheric water tower" over the Tibetan Plateau is $(25.76 \pm 3.83) \times 10^6$ kg s^{-1}, and the interannual variations in the reserve show a decreasing trend during Period I (1951–1973), but an increasing trend during Period II (1974–2022).

We found that the shift in the trend of the reserve in 1973 is consistent with the interannual variations in the corresponding AMO. During Period I, the reserve was only influenced by the AMO; however, during Period II the reserve was governed by the synergistic effects of climate forcings (the AMO, IOBW and ENSO) from the three oceans, including the North Atlantic, Indian, and Pacific Oceans. Our results also demonstrate that the dominant forcings for the interannual variations in the reserve were not fixed but have transitioned from the North Atlantic Ocean to the Pacific Ocean from around 1994. We postulate the main climatic forcing will likely revert back to the North Atlantic Ocean in the future. Clearly, the main forcing governing the "atmospheric water tower" reserve into the future deserves further study.

Our results highlight the synergistic effects of climate forcings from three oceans on the interannual variations in the "atmospheric water tower" reserve. Furthermore, our study provides new insights into the dominant climate forcings on the interannual variations in the reserve, marking a paradigm transition from a static to a dynamic framework. Our findings have important implications for the studies on weather, climate, and water resources in the Tibetan Plateau and surroundings.

CRediT authorship contribution statement

Pengjie Ren: Writing – review & editing, Writing – original draft, Visualization, Methodology, Investigation. **Wusheng Yu:** Writing – review & editing, Writing – original draft, Visualization, Supervision, Funding acquisition, Conceptualization. **Stephen Lewis:** Writing – review & editing, Writing – original draft. **Yaoming Ma:** Writing – original draft, Supervision, Resources, Funding acquisition, Conceptualization. **Yuanyuan Dang:** Formal analysis. **Lei Zhong:** Writing – original draft, Supervision, Resources, Methodology, Conceptualization. **Zhuanxia Zhang:** Visualization, Formal analysis. **Yong Liu:** Visualization, Methodology, Formal analysis. **Lun Luo:** Formal analysis. **Zhaowei Jing:** Formal analysis. **Jingyi Zhang:** Formal analysis. **Rong Guo:** Formal analysis. **Qiaoyi Wang:** Formal analysis. **Ziran Lei:** Formal analysis.

Declaration of competing interest

The authors declare that they have no known competing financial interests or personal relationships that could have appeared to influence the work reported in this paper.

Acknowledgements

This study was supported by the Second Tibetan Plateau Scientific Expedition and Research Program (STEP) (2024QZKK0400), the National Natural Science Foundation of China (U2442213), and the National Natural Science Foundation of China (42171122).

Data availability.

Data will be made available on request.

Appendix A. Supplementary data

Supplementary data to this article can be found online at https://doi.org/10.1016/j.jhydrol.2025.134785.

Data availability

Data will be made available on request.

References

Bolch, T., Kulkarni, A., Kääb, A., Huggel, C., Paul, F., Cogley, J.G., Frey, H., Kargel, J.S., Fujita, K., Scheel, M., Bajracharya, S., Stoffel, M., 2012. The State and Fate of Himalayan Glaciers. Science 336, 310–314. https://doi.org/10.1126/science.1215828.

Chen, X., You, Q., 2017. Effect of Indian Ocean SST on Tibetan Plateau precipitation in the early rainy season. J. Clim. 30, 8973–8985. https://doi.org/10.1175/JCLI-D-16-0814.1.

Chen, W., Liu, Y., Zhang, G., Yang, K., Zhou, T., Wang, J., Shum, C., 2022a. What controls lake contraction and then expansion in Tibetan Plateau's endorheic basin over the past half century? Geophys. Res. Lett. 49, e2022GL101200. https://doi.org/10.1029/2022GL101200.

Chen, Y., Wen, J., Liu, R., Zhou, J., Liu, W., 2022b. The characteristics of water vapor transport and its linkage with summer precipitation over the source region of the three Rivers. J. Hydrometeor. 23, 441–455. https://doi.org/10.1175/JHM-D-21-0095.1.

Feng, L., Zhou, T., 2012. Water vapor transport for summer precipitation over the Tibetan Plateau: Multidata set analysis. J. Geophys. Res. 117, D2011. https://doi.org/10.1029/2011JD017012.

Gao, K., Duan, A., Chen, D., 2021. Interdecadal summer warming of theTibetan Plateau potentially regulated by a sea surface temperature anomaly in the Labrador Sea. Int. J. Climatol. 41 (Suppl. 1), E2633–E2643. https://doi.org/10.1002/joc.6871.

Gao, Y., Cuo, L., Zhang, Y., 2014. Changes in moisture flux over the Tibetan Plateau during 1979–2011 and possible mechanisms. J. Clim. 27, 1876–1893. https://doi.org/10.1175/JCLI-D-13-00321.1.

Gao, Y., Wang, H., Li, S., 2013. Influences of the Atlantic Ocean on the summer precipitation of the southeastern Tibetan Plateau. J. Geophys. Res. Atmos. 118, 3534–3544. https://doi.org/10.1002/jgrd.50290.

He, Y., Tian, W., Huang, J., Wang, G., Ren, Y., Yan, H., Yu, H., Guan, X., Hu, H., 2021. The mechanism of increasing summer water vapor over the Tibetan Plateau. J. Geophys. Res. Atmos. 126, e2020JD034166. https://doi.org/10.1029/2020JD034166.

Immerzeel, W.W., van Beek, L.P., Bierkens, M.F., 2010. Climate change will affect the Asian water towers. Science 328, 1382–1385. https://doi.org/10.1126/science.1183188.

Jia, X., Chen, X., Dong, W., Ma, H., Ge, J., Qian, Q., 2025. Impact of Tibetan plateau warming amplification on the interannual variations in East Asia Summer precipitation. npj Clim. Atmos. Sci. 8, 29. https://doi.org/10.1038/s41612-025-00920-5.

Jing, Z., Yu, W., Schneider, A., Borsdorff, T., Landgraf, J., Lewis, S., Zhang, J., Tang, W., Ma, Y., Xu, B., Qu, D., 2021. Interannual variation in stable isotopes in water vapor over the northern Tibetan Plateau linked to ENSO. Geophys. Res. Lett. 48, e2021GL092708. https://doi.org/10.1029/2021GL092708.

Li, X., Long, D., Scanlon, B.R., Mann, M.E., Li, X., Tian, F., Sun, Z., Wang, G., 2022a. Climate change threatens terrestrial water storage over the Tibetan Plateau. Nat. Clim. Chang. 12, 801–807. https://doi.org/10.1038/s41558-022-01443-0.

Li, X., Wu, P., Ding, Y., Liu, Y., Li, Q., 2022b. Spatial-temporal variation of precipitation recycling over the Tibetan Plateau under climate warming. Atmos. Res. 280, 106431. https://doi.org/10.1016/j.atmosres.2022.106431.

Lin, H., You, Q., Zhang, Y., Jiao, Y., Fraedrich, K., 2016. Impact of large-scale circulation on the water vapour balance of the Tibetan Plateau in summer. Int. J. Climatol. 36, 4213–4221. https://doi.org/10.1002/joc.4626.

Liu, Y., Chen, H., Li, H., Zhang, G., Wang, H., 2021. What induces the interdecadal shift of the dipole patterns of summer precipitation trends over the Tibetan Plateau? Int. J. Climatol. 41, 5159–5177. https://doi.org/10.1002/joc.7122.

Liu, Y., Wang, H., Chen, H., Zhang, Z., Li, H., Liu, B., 2023. Anthropogenic forcing and Pacific internal variability-determined decadal increase in summer precipitation over the Asian water tower. npj Clim. Atmos. Sci. 6, 38. https://doi.org/10.1038/s41612-023-00369-4.

Ma, Y., Lu, M., Chen, H., Pan, M., Hong, Y., 2018. Atmospheric moisture transport versus precipitation across the Tibetan Plateau: a mini-review and current challenges. Atmos. Res. 209, 50–58. https://doi.org/10.1016/j.atmosres.2018.03.015.

Meng, D., Qing, D., Kong, F., Yin, Z., Li, Y., Liu, J., 2020. Spatio-temporal variations of water vapor budget over the Tibetan Plateau in summer and its relationship with the Indo-Pacific Warm Pool. Atmosphere 11, 828. https://doi.org/10.3390/atmos11080828.

Ropelewski, C.F., Jones, P.D., 1987. An extension of the Tahiti-Darwin Southern Oscillation Index. Mon. Wea. Rev. 115, 2161–2165. https://doi.org/10.1175/1520-0493(1987)115<2161:AEOTTS>2.0.CO;2.

Sun, B., Zhu, Y., Wang, H., 2011. The recent interdecadal and interannual variation of water vapor transport over eastern China. Adv. Atmos. Sci. 28, 1039–1048. https://doi.org/10.1007/s00376-010-0093-1.

Sun, J., Yang, K., Guo, W.D., Wang, Y., He, J., Lu, H., 2020. Why has the Inner Tibetan Plateau become wetter since the mid-1990s? J. Clim. 33, 8507–8522. https://doi.org/10.1175/JCLI-D-19-0471.1.

Sun, L., Yang, Y., Fu, Y., Zhang, X., Zhong, L., Zhao, C., Ma, M., 2022. Summertime atmospheric water vapor transport between Tibetan Plateau and its surrounding regions during 1990–2019: Boundary discrepancy and interannual variation. Atmos. Res. 275, 106237. https://doi.org/10.1016/j.atmosres.2022.106237.

Takaya, K., Nakamura, H., 2001. A formulation of a phase-independent wave-activity flux for stationary and migratory quasigeostrophic eddies on a zonally varying basic flow. J. Atmos. Sci. 58, 608–627. https://doi.org/10.1175/1520-0469(2001)058<0608:AFOAPI>2.0.CO;2.

Trenberth, K.E., 1991. Climate diagnostics from global analyses: conservation of mass in ECMWF analyses. J. Clim. 4 (7), 707–722. https://doi.org/10.1175/1520-0442(1991)004<0707:CDFGAC>2.0.CO;2.

Wan, B., Gao, Z., Chen, F., Lu, C., 2017. Impact of Tibetan Plateau surface heating on persistent extreme precipitation events in Southeastern China. Mon. Wea. Rev. 145, 3485–3505. https://doi.org/10.1175/MWR-D-17-0061.1.

Wang, H., Liu, G., Wang, S., He, K., 2021. Precursory signals (SST and soil moisture) of summer surface temperature anomalies over the Tibetan Plateau. Atmosphere 12 (2), 146. https://doi.org/10.3390/atmos12020146.

Wang, H., Zhao, P., 2022. Spatiotemporal variation of water vapor budget over the Tibetan Plateau and its regulation on precipitation. J. Trop. Meteorol. 28 (2), 194–206. https://doi.org/10.46267/j.1006-8775.2022.015.

Wang, L., Liu, H., Zhong, X., Zhou, J., Zhu, L., Yao, T., Xie, C., Ju, J., Chen, D., Yang, K., Zhao, L., Lu, S., Khanal, S., Jin, J., Liu, W., Liu, B., Du, Y., Yao, X., Lei, Y., Zhang, G., Nepal, S., 2022. Domino effect of a natural cascade alpine lake system on the Third Pole. Proc. Natl. Acad. Sci. Nexus 1, 1–9. https://doi.org/10.1093/pnasnexus/pgac053.

Wang, Z., Duan, A., Yang, S., Ullah, K., 2017. Atmospheric moisture budget and its regulation on the variability of summer precipitation over the Tibetan Plateau. J. Geophys. Res. Atmos. 122, 614–630. https://doi.org/10.1002/2016JD025515.

Wang, Z., Lei, Y., Che, H., Wu, B., Zhang, X., 2024. Aerosol forcing regulating recent decadal change of summer water vapor budget over the Tibetan Plateau. Nat. Commun. 15, 2233. https://doi.org/10.1038/s41467-024-46635-8.

Wei, Y., Yu, H., 2024. The interdecadal weakening of the relationship between Indian Ocean sea surface temperature and summer precipitation in Central Asia. Geophys. Res. Lett. 51, e2023GL107371. https://doi.org/10.1029/2023GL107371.

Xu, K., Zhong, L., Ma, Y., Zou, M., Huang, Z., 2020. A study on the water vapor transport trend and water vapor source of the Tibetan Plateau. Theor. Appl. Climatol. 140, 1031–1042. https://doi.org/10.1007/s00704-020-03142-2.

Xu, X., Lu, C., Shi, X., Gao, S., 2008. World water tower: an atmospheric perspective. Geophys. Res. Lett. 35 (20), 525–530. https://doi.org/10.1029/2008GL035867.

Xu, X., Zhao, T., Lu, C., Guo, Y., Chen, B., Liu, R., Li, Y., Shi, X., 2014. An important mechanism sustaining the atmospheric "water tower" over the Tibetan Plateau. Atmos. Chem. Phys. 14, 11287–11295. https://doi.org/10.5194/acp-14-11287-2014.

Yan, H., Huang, J., He, Y., Liu, Y., Wang, T., Li, J., 2020. Atmospheric water vapor budget and its long-term trend over the Tibetan Plateau. J. Geophys. Res. Atmos. 125, e2020JD033297. https://doi.org/10.1029/2020JD033297.

Yang, L., Li, K.B., Shen, Y., Tian, F.Q., 2022. Flood seasonality over the third pole region modulated by upper level moisture transport. Earth's Future 10 (9), 1–10. https://doi.org/10.1029/2022EF002828.

Yang, J., Liu, Q., Liu, Z., Wu, L., Huang, F., 2009. Basin mode of Indian Ocean sea surface temperature and Northern Hemisphere circumglobal teleconnection. Geophys. Res. Lett. 36, L19705. https://doi.org/10.1029/2009GL039559.

Yu, J., Li, Q., Ding, Y., Zhang, J., Wu, Q., Shen, X., 2022. Long-term trend of water vapor over the Tibetan Plateau in boreal summer under global warming. Sci. China Earth Sci. 65 (4), 662–674. https://doi.org/10.1007/s11430-021-9874-0.

Zhang, C., Tang, Q., Chen, D., 2017a. Recent changes in the moisture source of precipitation over the Tibetan Plateau. J. Clim. 30, 1807–1819. https://doi.org/10.1175/JCLI-D-15-0842.1.

Zhang, Q., Shen, Z., Pokhrel, Y., Farinotti, D., Singh, V.P., Xu, C., Wu, W., Wang, G., 2023. Oceanic climate changes threaten the sustainability of Asia's water tower. Nature 615, 87–93. https://doi.org/10.1038/s41586-022-05643-8.

Zhang, W., Zhou, T., Zhang, L., 2017b. Wetting and greening Tibetan Plateau in early summer in recent decades. J. Geophys. Res. Atmos. 122, 5808–5822. https://doi.org/10.1002/2017JD026468.

Zhang, Y., Li, B., Liu, L., Zheng, D., 2021. Redetermine the region and boundaries of Tibetan Plateau. Geogr. Res. 40, 1543–1553. https://doi.org/10.11821/dlyj020210138.

Zhao, Y., Xu, C., Yu, X., Liu, Y., Ji, X., 2025. Atlantic oceanic droughts do not threaten Asian water tower. Nature 638, E13–E15. https://doi.org/10.1038/s41586-024-08357-1.

Zhao, Y., Xu, X., Chen, B., Wang, Y., 2016. The upstream "strong signals" of the water vapor transport over the Tibetan Plateau during a heavy rainfall event in the Yangtze River Basin. Adv. Atmos. Sci. 33, 1343–1350. https://doi.org/10.1007/s00376-016-6118-7.

Zhao, Y., Zhou, T., 2021. Interannual variability of precipitation recycle ratio over the Tibetan Plateau. J. Geophys. Res. 126, e2020JD033733. https://doi.org/10.1029/2020JD033733.

Zhou, C., Zhao, P., Chen, J., 2019. The interdecadal change of summer water vapor over the Tibetan Plateau and associated mechanisms. J. Clim. 32, 4103–4119. https://doi.org/10.1175/JCLI-D-18-0364.1.

Zhu, Q., Liu, Y., Shao, T., Luo, R., Tan, Z., 2021. Role of the Tibetan Plateau in northern drought induced by changes in the subtropical westerly jet. J. Clim. 34, 4955–4969. https://doi.org/10.1175/JCLI-D-20-0799.1.